Fluorescence microscopy three-dimensional depth variant point spread function interpolation using Zernike moments

Elie Maalouf, Bruno Colicchio, Alain Dieterlen

Fluorescence microscopy three-dimensional depth variant point spread function interpolation using Zernike moments

Elie Maalouf,* Bruno Colicchio, and Alain Dieterlen

Modélisation, Intelligence, Processus et Systèmes Laboratory, Université de Haute Alsace, Institut Universitaire de Technologie de Mulhouse, 61, rue Albert Camus, 68093 Mulhouse Cedex, France
**Corresponding author: elie.el-maalouf@uha.fr*

Received April 11, 2011; revised July 12, 2011; accepted July 13, 2011;
posted July 18, 2011 (Doc. ID 145371); published August 23, 2011

In three-dimensional fluorescence microscopy the point spread function (PSF) changes with depth, inducing errors in the restored images when these variations are neglected during the deconvolution of thick specimens. Some deconvolution algorithms have been developed to take the depth variations of the PSF into consideration. For these algorithms, the accuracy of the estimated structures depends on the knowledge of the PSF at various depths. We propose an alternative to measuring all required PSFs at different depths. The needed PSFs are interpolated from a limited measured PSF set using a method based on Zernike moments. The proposed method offers the possibility to obtain an accurate PSF interpolation at different depths using only a few measured ones. © 2011 Optical Society of America

OCIS codes: 100.2000, 100.6890, 180.2520, 100.1830.

1. INTRODUCTION

Wide-field fluorescence microscopy is the method of choice for studying living cells, due to its ability to show specifically labeled structures within a complex environment. Combined with the computational optical sectioning, it provides fast three-dimensional (3D) measurements of biological structures.

Unfortunately, the image intensities are corrupted by the fact that upon illumination all fluorescently labeled structures emit light whether they are in focus or not. This means that a 3D image is always blurred by the contribution of light from out of focus structures. This phenomenon manifests itself as blurred data [1].

Many deconvolution techniques have been developed to reverse this phenomenon and restore an estimation of the original object using the point spread function of the optical system [2]. These techniques assume that the point spread function (PSF) is shift invariant into the object space [3–5]. In optical sectioning fluorescence microscopy, the point spread function may change significantly along the optical axis as the depth increases [6]. New approaches taking the space noninvariance of the PSF into account have been developed [7–10]; in such algorithms the knowledge of a large number of PSFs at different depth positions is mandatory and the number of used PSFs directly affects the deconvolution quality [11].

In order to supply the needed PSF, mathematical models have been developed [12,13] which calculate a theoretical PSF for a given system using a set of optical parameters. However, a mathematical model fails to take into account the aberrations of the entire real optical system [14], especially the aberrations which are induced by the refractive index of the specimen [15]. Some techniques attempt to adjust the parameters of the mathematical model used to be as close as possible to the actual measurement values either by recovering data from an experimental PSF [16] or by proposing a simplified model with a restrained set of parameters that can be adjusted using two measured PSFs and a maximum likelihood [17]. Kam *et al.* proposed to estimate the 3D refractive index variations by using Nomarski differential interference contrast microscopy and use this information to model PSFs that take into account the refractive index variations induced by the specimen [18]. PSFs at various depths can also be calculated by a method described by Hanser *et al.* [19], where the pupil function of a microscope is computationally estimated from a measured point spread function using phase retrieval algorithms.

The most accurate way to obtain the PSF of a system at a certain spatial point is by measuring a subresolution fluorescent bead at that point which approximates a point source. The use of a measured PSF offers the advantage of taking into account the aberrations of the entire optical system. Some measurements have been made using subresolution beads either embedded in optical cement [14] or fixed to a tilted surface [1] or on a 1 mm sapphire bead [19]. Other authors try to identify and extract small structures in the imaged specimen that can be considered as a PSF [20,21]. These techniques give a limited number of randomly positioned PSFs. Thus, in an attempt to obtain more PSFs at a more controlled depth, optical tweezers attached to an epifluorescence microscope has been proposed [11]. This method allows the measurement of a depth variant PSF by axially shifting a small bead using the optical tweezers. According to the author, this method is not suitable for very deep specimens where an alternative technique will have to be developed.

Because of the complexity in modeling precisely or measuring the 3D PSF at different depths, an alternative method is proposed in order to obtain a faithful PSF estimation at any

needed depth from a limited number of measured ones using an interpolation technique. The proposed technique provides the needed PSF for optimal deconvolution results in a noninvariance assumption using a minimal number of measured ones. The PSF variations are quantified by decomposing the image into a set of descriptors representing the PSF properties using the image moments theory and the Zernike polynomials as a basis (generally known as Zernike moments). The known 3D PSFs are decomposed using pseudo-3D Zernike moments; their variations are then fitted into polynomial functions that can be used to interpolate a new description for a missing PSF at any depth.

2. PSF REPRESENTATION WITH ZERNIKE MOMENTS

A. General Moment Theory

Moments are scalar quantities used to characterize a function and to capture its significant features. A set of moments computed from a digital image generally represents global characteristics of the image and provides a lot of information about different types of geometrical features of the image. For these reasons, image moments are widely used in computer vision and robotics for object identification techniques.

From the mathematical point of view, moments are projections of a function onto a polynomial basis. An image can be considered as a two-dimensional continuous real function $f(x,y)$ defined over a two-dimensional (2D) plane in a domain noted ς, where the value denotes the pixel intensity at location (x,y). A general definition of the moment function Φ_{pq} of an image $f(x,y)$, where p and q are nonnegative integers and $(p+q)$ is the order, can be written as

$$\Phi_{pq} = \iint_{\varsigma} \Psi_{pq}(x,y) f(x,y)\mathrm{d}x\mathrm{d}y, \qquad p,q = 0,1,2,3.... \quad (1)$$

The function $\Psi_{pq}(x,y)$ is continuous over the domain ς and is known as the moment weighting kernel or the basis set. Usually p and q denote the degrees of the coordinates x, y, respectively, as defined inside the function and depending on the polynomial basis used.

B. Zernike Moments

Zernike polynomials are widely used as a basis function of image moments. They have been proven to be superior to other moment functions [22,23] in terms of their feature representation capabilities and robustness in the presence of noise and offer a good reconstruction of the image [24]. Their orthogonal property helps to achieve a near zero value in terms of the redundancy measure in a set of moment functions. Thus, moments of different orders correspond to independent characteristics of the image [25]. An accurate representation of a PSF can then be achieved by using Zernike moments, since they offer a compact representation where low-order coefficients represent typical aberrations, while noise is represented in higher order coefficients [26].

Zernike moments are based on a set of complete and orthogonal functions defined over a polar coordinate space, inside a unit circle. The 2D Zernike moment A_{pq} of order p and repetition q of a continuous function $f(\rho,\theta)$ is defined as

$$A_{pq} = \frac{1+p}{\pi} \int_0^1 \int_{-\pi}^{\pi} f(\rho,\theta)[V_{pq}(\rho,\theta)]\rho\mathrm{d}\rho\mathrm{d}\theta$$
$$\begin{cases} p = 0,1,2,...\infty \\ q \in Z \\ p - |q| \text{is even}, |q| < p \end{cases}. \quad (2)$$

The Zernike polynomial $V_{pq}(\rho,\theta)$ is defined as

$$V_{pq}(\rho,\theta) = R_{pq}(\rho)e^{-iq\theta}, \quad (3)$$

where $R_{pq}(\rho)$ is the orthogonal radial polynomial defined as

$$R_{pq}(\rho) = \sum_{s=0}^{(p-|q|)/2} (-1)^s \frac{(p-s)!}{s!\left(\frac{p+|q|}{2}-s\right)!\left(\frac{p-|q|}{2}-s\right)!}\rho^{p-2s}. \quad (4)$$

Since Zernike moments are defined in terms of polar coordinates (ρ,θ) with $\rho \le 1$, their computation requires a linear transformation of the image coordinates to a suitable domain inside a unit circle [23]. As 2D PSFs are considered as Airy disks, the transformation $(0;N-1) \rightarrow^{\text{yields}} (-1;+1)$ will be used (Fig. 1).

Where $x = \frac{i-i_c}{N}$ and $y = \frac{j-j_c}{N}$ with i_c, j_c as the Cartesian coordinate of the center of the unit circle. Then $\rho = \sqrt{x^2+y^2}$ is the length of the vector from the origin to the mapped pixel (x,y) into the unit circle, $\theta = \tan^{-1}\frac{y}{x}$ is the angle between the vector and the x axis, and $x^2+y^2 \le 1$.

The discrete approximation of Zernike moments is expressed as follows:

$$A_{pq} = \tau_{(N,p)} \sum_{x=0}^{N-1}\sum_{y=0}^{N-1} f(\rho,\theta)V(\rho,\theta) \quad \{\rho = x^2+y^2 \le 1\}. \quad (5)$$

$\tau_{(D,p)}$ is a normalization factor, which is the number of pixels located in the unit circle by the mapping transform, and corresponds to the area π of a unit circle in the continuous domain.

The image intensity can then be expressed using Zernike polynomials over the unit circle as

$$f(\rho,\theta) = \sum_{p=0}^{\infty}\sum_{q=0}^{p} A_{pq}V_{pq}(\rho,\theta), \quad (6)$$

with Zernike moments A_{pq} calculated over the same unit circle.

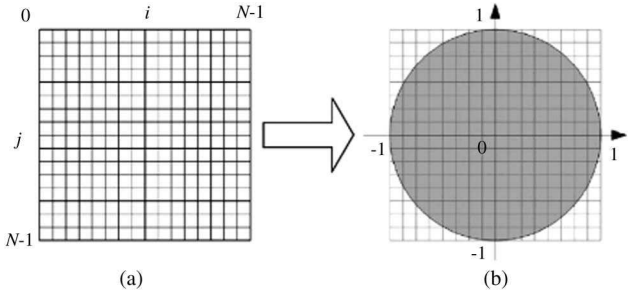

Fig. 1. Mapping transform between the Cartesian coordinates of an image to the polar coordinates inside a unit circle.

However, the reconstruction of an image using an infinite number of moments is computationally impossible; therefore, this expansion is truncated to a finite order $P_{\max}$ and considered as an optimum approximation to the original image function. $P_{\max}$ is fixed at 45 according to the experimental results of a previous work [25].

The estimated reconstructed image $\widehat{f}$ is given as

$$\widehat{f}(\rho,\theta)=\sum_{p=0}^{p_{\max}}\sum_{q=0}^{p}A_{pq}V_{pq}(\rho,\theta). \tag{7}$$

This estimate can be easily computed using an expansion with real valued functions as given below:

$$\widehat{f}(\rho,\theta)=\sum_{p=0}^{N_{\max}}\sum_{q>0}^{p}(C_{pq}\cos q\theta + S_{pq}\sin q\theta)R_{pq}(\rho)+\frac{C_{p0}}{2}R_{p0}(\rho), \tag{8}$$

where C_{pq} and S_{pq} are the real and imaginary parts of A_{pq} with

$$\begin{aligned}C_{pq}&=2\mathrm{Re}(A_{pq})\\&=\frac{2p+2}{\pi}\int_0^1\int_{-\pi}^{\pi}f(\rho,\theta)R_{pq}(\rho)\cos(q\theta)\rho\mathrm{d}\rho\mathrm{d}\theta\\S_{pq}&=-2\mathrm{Im}(A_{pq})\\&=\frac{-2p-2}{\pi}\int_0^1\int_{-\pi}^{\pi}f(\rho,\theta)R_{pq}(\rho)\sin(q\theta)\rho\mathrm{d}\rho\mathrm{d}\theta.\end{aligned} \tag{9}$$

C. Describing PSF with Zernike Moments

In our work, a 3D PSF is considered as a stack of 2D Airy patterns (Fig. 2) and the decomposition of a 3D PSF using Zernike moments is reduced to the decomposition of each slice (centered on the optical axis of the 3D PSF). Then the reconstruction is done by reconstructing each slice apart. For a given order p, repetition q, and a slice n, one can write

$$\begin{aligned}C_{pq}^{n}&=2\mathrm{Re}(A_{pq}^{n})=\frac{2p+2}{\pi}\sum_x\sum_y f_{(\rho,\theta)}^{n}R(\rho)\cos(q\theta),\\S_{pq}^{n}&=-2\mathrm{Im}(A_{pq}^{n})=\frac{-2p-2}{\pi}\sum_x\sum_y f_{(\rho,\theta)}^{n}R(\rho)\sin(q\theta),\end{aligned} \tag{10}$$

where $\rho=\sqrt{x^2+y^2}\le 1$ and $\theta=\tan^{-1}\frac{y}{x}$.

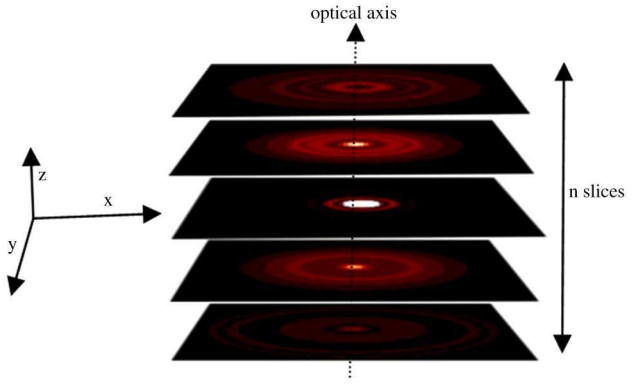

Fig. 2. (Color online) 3D PSF representation—all slices are centered the same way in the unit circle (the center is calculated using the Airy disk).

By applying Eq. (8), the plane n can be estimated from C_{pq}^{n} and S_{pq}^{n} as

$$\widehat{f}^{n}(\rho,\theta)=\sum_{p=0}^{P_{\max}}\sum_{q>0}^{p}(C_{pq}^{n}\cos(q\theta)+S_{pq}^{n}\sin(q\theta))R_{pq}(\rho)+\frac{C_{p0}^{n}}{2}R_{p0}(\rho), \tag{11}$$

the term $R(\rho)$ can be calculated once and used for all planes of the PSF (or any PSF of same dimensions).

Each PSF plane is then represented by two sets of Zernike moment components (Re and Im) with $p_{\max}$ as a maximal optimal order. A 3D PSF having n plane at depth k can be represented using Zernike moments as follows:

$$Z_k=[B_{00}^{k}\quad\ldots\quad B_{pq}^{k}]=\begin{bmatrix}A_{00}^{1}&\cdots&A_{pq}^{1}\\\vdots&\ddots&\vdots\\A_{00}^{n}&\cdots&A_{pq}^{n}\end{bmatrix}. \tag{12}$$

For the rest of this article we will refer to this representation Z_k as pseudo-3D Zernike moments of the PSF at depth k.

D. Describing Rotationally Symmetric PSF with Zernike Moments

For a rotationally symmetric PSF along the optical axis, the S_{pq}^{n} is equal to zero and only the real part (C_{pq}^{n}) of Zernike moments needs to be considered:

$$A_{pq}^{n}=\frac{1}{2}C_{pq}^{n}. \tag{13}$$

And the simplified version of Eq. (8) can be written as

$$\widehat{f}^{n}(\rho,\theta)=\sum_{p=1}^{N_{\max}}\sum_{q>0}^{p}C_{pq}^{n}\cos(q\theta)R_{pq}(\rho)+\frac{C_{p0}^{n}}{2}R_{p0}(\rho). \tag{14}$$

3. ANALYSIS OF A MOMENT COMPONENT VARIATION

To analyze the variation of a Zernike moments component along the depth of the PSF, the known PSF is described using pseudo-3D Zernike moments and the 3D matrix $MZ(a,n,k)$ is formed, where each plane holds $Z_k\{1\le k\le K\}$. In the matrix $MZ(a,n,k)$, each plane represents a PSF at depth k, where each line holds the component of Zernike moments representation of the plane n with index a.

To get a specific pseudo-3D moment variation, V_{an} is constructed:

$$V_{an}(i)=MZ(a,n,i)\quad\{1\le i\le K\}. \tag{15}$$

The moment index a is related to the moment order and repetition p, q by the following equation:

$$a=\begin{cases}\left(\frac{p-1}{2}+1\right)\left(\frac{p-1}{2}+2\right)+\frac{q}{2}+1 & p\text{ is even}\\\left(\frac{p-2}{2}+1\right)\left(\frac{p-2}{2}+2\right)+\frac{p-1}{2}+\frac{q}{2}+2 & p\text{ is odd}\end{cases}. \tag{16}$$

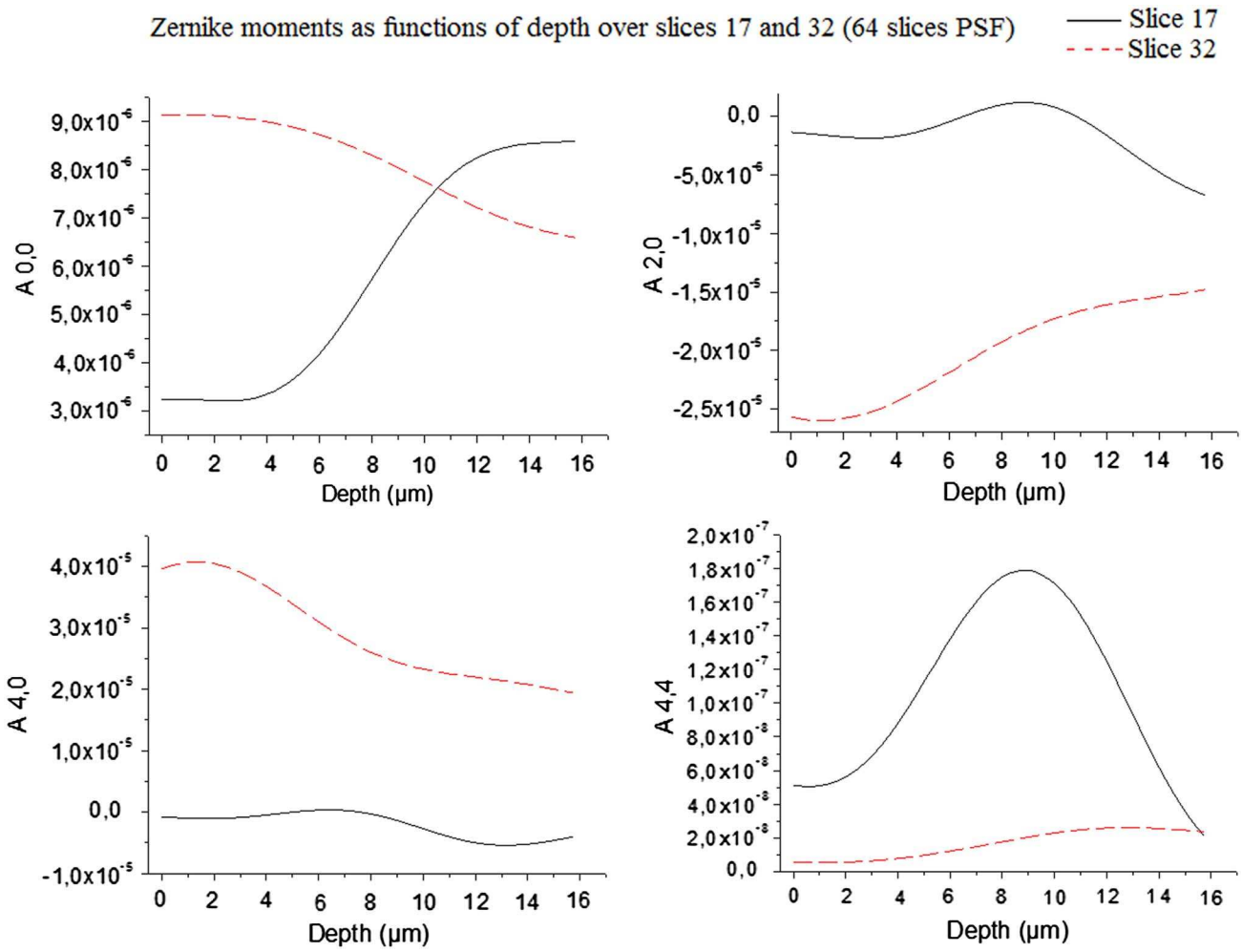

Fig. 3. (Color online) Four Zernike moments variations over the 17th plane and the 32nd, along the depth (0 μm–15.75 μm).

Figure 3 shows the C_{pq} variation for a simulated set of the PSF over two different planes using the vectorial model [27] for a wide-field microscope (rotationally symmetric PSF).

4. POLYNOMIAL FITTING AND INTERPOLATION

In the rest of this article we will consider the rotational symmetric PSF case for the sake of simplicity. In the general case, the process remains the same but must be applied on both the C_{pq} and S_{pq} components.

The changes in the pseudo-3D Zernike moments component can be estimated using polynomial fittings. Each $V_{an}(i)$ is estimated by a polynomial function; thereby the MZ 3D matrix is transformed to a 2D matrix of polynomial functions. This transformation can be written as

$$MZ(a,n,k) \overset{\text{Poly Fit}}{\rightarrow} VZ(a,n) = \begin{pmatrix} p_{00} & \cdots & p_{a0} \\ \vdots & \ddots & \vdots \\ p_{0n} & \cdots & p_{an} \end{pmatrix}, \qquad (17)$$

where p_{an} is the polynomial function representing the variation through the depth of the moment of index a in the plane n.

Having polynomials describing each moment component variation, it becomes straightforward to interpolate the whole set of pseudo-3D moments values at a certain depth and construct an estimate of the PSF using Eq. (11).

Based on K PSFs at various depths, the interpolation process can be described as follows:

- K PSF at various depths are described using pseudo-3D Zernike moments, and $MZ(a,p,k)$ is formed.
- MZ is transformed to the polynomial functions matrix $VZ(a,p)$ using a polynomial fitting.
- For each needed depth value the entire set of 3D-pseudo Zernike values are estimated using VZ functions.
- The estimated PSF are constructed.

5. DISCUSSION AND RESULTS

The tests aiming to validate the process are carried over simulated PSFs in a volume of $64 \times 64 \times 64$ voxels (voxel size is 0.068 μm in the lateral axis and 0.25 μm in the optical axis), computed using Török and Varga vectorial model modified by Haeberlé [27] (objective 100×, NA = 1.4, emission wavelength of 630 nm, oil refractive index of 1.515, specimen immersion medium refractive index of 1.33). Gaussian noise is added, resulting in images with different signal-to-noise ratios (SNRs) (30 dB and 20 dB) to demonstrate the interpolation robustness.

A. Pseudo-3D Reconstruction

In [28,29], one can find a discussion about the problem of estimating a function on the unit circle given discrete and noisy data recorded on a regular square grid. The higher the maximum order $P_{\max}$ used, the better the accuracy of the reconstructed image. The value of $P_{\max}$ is actually limited by the computational method used for factorial evaluation in Eq. (4).

In order to evaluate the reconstruction accuracy of a 3D PSF using the pseudo-3D Zernike moments according to Eq. (11), two PSFs at depth 0.5 and 10 μm are used. Reconstructions with a maximum Zernike order of $P_{\max} = 45$ are done in noise-free conditions and with a SNR of 20 dB. The error criterion used is the 3D correlation coefficient according to the formula

$$r_p = \frac{\sum_{i=0}^{i<N}(X_i - \bar{X})(Y_i - \bar{Y})}{\sqrt{\sum_{i=0}^{i<N}(X_i - \bar{X})^2 \sum_{i=0}^{i<N}(Y_i - \bar{Y})^2}}. \quad (18)$$

The reconstructions have a coefficient correlation of up to 0.99 relative to the calculated noiseless image. In the presence of noise, the correlation coefficient increases from 0.70 in the case of the noisy original image with a SNR of 20 db at 0.5 μm of depth (Fig. 4) to 0.85 in the case of the constructed one, this coefficient increases from 0.82 to 0.95 for the PSF at 10 μm of depth (Fig. 5).

The correlation coefficient is close to but not equal to 1, due to the limited number of Zernike orders used in the reconstruction. On the other hand, in the presence of noise the order number limitation induces a filtering effect, while conserving the main features of the PSF.

B. Fitting Order Evaluation

The algorithm uses the polynomial fitting for interpolation, so it is quite obvious that one of the basic conditions is to have values uniformly scattered over the interpolation area.

The fitting order depends on the number of PSFs used as $f_{\text{ord}} \le K - 1$, where f_{ord} is the fitting order used and K is the number of known PSFs. Furthermore, when the image is corrupted with noise, the Zernike moments variations present local irregularities, and fitting them with polynomials of a high order will introduce significant errors into the interpolation, as the high order polynomial will try to follow the irregularities and deviate widely at some regions.

As an illustration, in our simulation the fitting order used is five and six calculated the PSFs used for interpolation. The

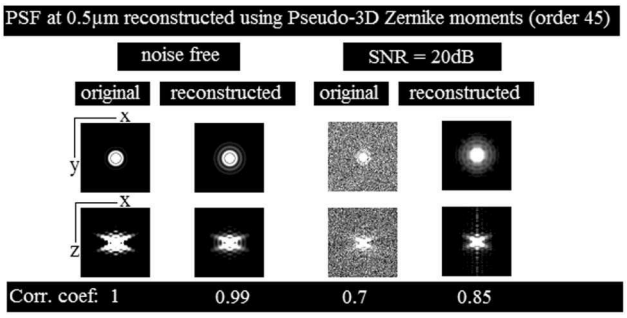

Fig. 4. Original (calculated) PSF at 0.5 μm of depth and the reconstructed one using pseudo-3D Zernike with an order of 45. The contrast was deliberately modified in order to highlight low intensity structures.

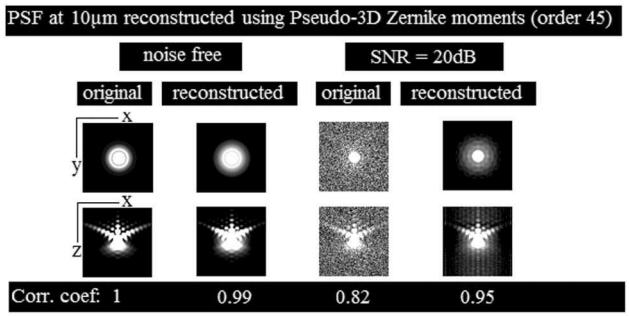

Fig. 5. Original (calculated) PSF at 10 μm of depth and the reconstructed one using pseudo-3D Zernike with 45 orders. The contrast was deliberately modified in order to highlight low intensity structures.

known PSFs are at locations 0–3–6–9–12–15.75 μm. The PSFs are interpolated at positions extending from 0 till 15.75 μm with steps of 0.25 μm and are compared with calculated noise-free PSFs using the correlation coefficient as resemblance criteria. The test is carried out with noise-free PSFs and with PSFs degraded with Gaussian noise of 30 and 20 dB SNR. Results are presented in Fig. 6. The polynomial fitting order used is five, and the Zernike maximal decomposition order is 45.

As can be seen in Fig. 6, the interpolated PSF reach a correlation coefficient at 0.98 with a 30 dB SNR, and drops to a mean of 0.87 at 20 dB SNR. A qualitative representation of interpolated PSFs at 7 μm can be seen at Fig. 7.

C. Experimental Part

For this experimental part, a sample is prepared using fluorescent nanobeads (FluoSphere Molecular Probes) fixed into a 30 μm thick polymer layer; the beads are 100 nm in diameter and their emission wavelength is around 630 nm.

The beads used are Latex FluoSpheres from Molecular Probes. These particles (supplied as aqueous suspensions) are added to a mix containing a photocrosslinkable formulation and a linear polymer binder in order to ensure their dispersion. The mix is actually an aqueous solution of

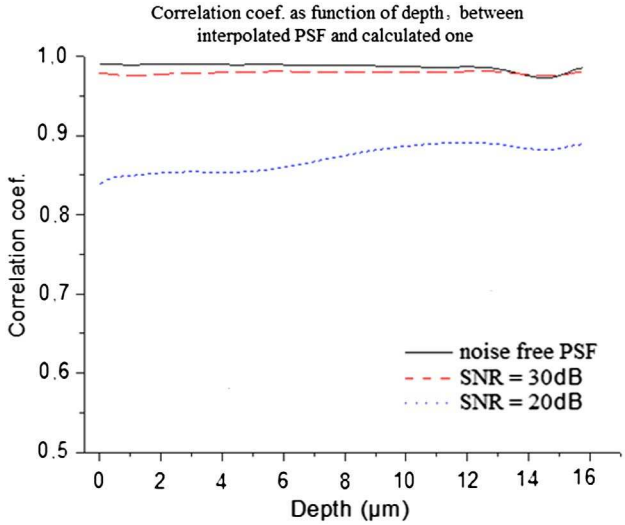

Fig. 6. (Color online) Correlation coefficient as a function of PSF depth, between the interpolated PSF (using six PSF, noise-free and a SNR of 30, 20 dB) at 0, 3, 6, 9, 12, and 15.75 μm) and the calculated one.

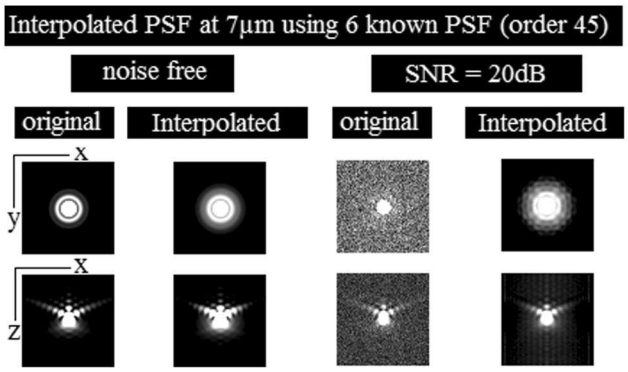

Fig. 7. Interpolated PSF at 7 μm using six known PSFs, from left to right: noise-free, 20 dB Gaussian noise (the originals are given as comparison references).

polyvinylalcohol, methyldiethanolamine (MDEA), vinylpyrrolidone (VP), methylene bisacrylamide (MBA), and Quantacure 4719 (QTX from Ward Blenkinsop).

1.5 ml of this formulation were deposited on a microscope glass slide and then irradiated with a UV source in a moister controlled environment. A standard glass cover slip is then glued to the top by photocuring a liquid resin specially designed to perfectly adhere to the surface of the specimen, to be easily activated through the glass cover (365 nm) and to match the refractive index of the polymer media used to embed the nanoparticles (typ. 1.475) [25].

The acquisitions are made with a wide field epifluorescence microscope based on an Olympus BX51, modified to acquire 3D images using computational optical sectioning. An oil immersion ($n_{\text{oil}} = 1.515$) 100× objective having a NA of 1.4 is mounted on a piezoelectric platform capable of moving along the optical axis in a range of −50 μm and +50 μm; the axial step is set to be 0.25 μm. The images are captured using a cooled CCD (CoolSnap HQ2) camera having 6.45×6.45 μm pixels yielding a lateral resolution of 0.064 μm, and digitized using 14 bits depth (16 bits images). Full frame images are acquired starting from the lowest point of the piezo range (−50 μm) up to 128 slices (0.25 μm axial resolution).

The first plane is considered as the relative origin of the depth (the relative 0 μm). Individual well-separated beads are manually selected and seven PSFs has been extracted at relative depths 4, 8, 15.75, 18.25, 20.75, 22.75, and 25.75 μm. These PSFs are centered in a $64 \times 64 \times 64$ voxels volume and then normalized. Figure 8 shows two extracted PSFs at depth 4 μm (Fig. 8(a)) and 25.75 μm (Fig. 8(b)). One can notice a change in the elongation along the optical axis. This asymmetry is not as strong as the one shown in the simulated images described before. It is actually due to the high refractive index of the embedding polymer (around 1.45) closer to the immersion medium (oil) refractive index (1.515) then

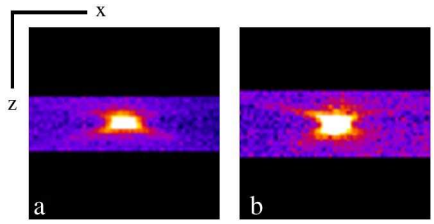

Fig. 8. (Color online) Extracted PSF at a relative depth of (a) 4 μm and (b) 25.75 μm.

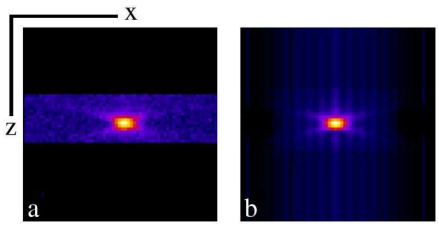

Fig. 9. (Color online) Interpolated PSF at a relative depth of (b) 18.25 μm compared to (a) the measured one at the same position .

the water (1.33) used in the simulation. Furthermore, the acquired images present a low SNR due to the background fluorescence.

In order to test the efficiency of the Zernike interpolation, six PSFs are used and the 7th is interpolated and then compared with the known measured one. This test is applied to the PSF at 18.25 μm. A general interpolation method is considered (real and imaginary parts are used), 45 Zernike order and a polynomial fitting order of five are used.

Figure 9 shows the interpolated PSF at a relative depth of 18.25 μm (Fig. 9(b)) in comparison with the measured one at the same position (Fig. 9(a)), one can see that the main PSF's features are successfully estimated.

6. CONCLUSION AND PERSPECTIVE

Taking into account the depth variant PSF problem into the image formation process and the deconvolution applications is an increasing field of research. The literature shows some techniques in order to provide the necessary PSFs for such a model.

In this context, an effective interpolation technique based on Zernike moments has been developed. This technique allows interpolating PSFs needed at various depths, using a restricted number of known (measured) PSFs only. This interpolation technique efficiency was validated on simulated and measured PSFs with 100 nm fluobeads imbedded in polymers.

This technique may also be used to interpolate PSFs when an other parameter changes such as the light wave length or the oil refractive index.

The process is implemented using java language as an ImageJ plugin, soon to be published on ImageJ wiki. Using a 2.4 GHz personal computer with 4 GBytes of random-access memory and 64 bits Java Virtual Machine, the processing time for the interpolation tests above were around one or two minutes. The interpolation process has been implemented using a basic algorithm for computing Zernike polynomials and moments. This time can be largely optimized by using advanced Zernike computation techniques [30,31].

ACKNOWLEDGMENTS

We would like to thank the Department de Photo-chimie General for their help in preparing the beads samples, also the ANR DIAMOND (http://www-syscom.univ-mlv.fr/ANRDIAMOND/). The ANR (Agence Nationale de la Recherche) is the French National Research Agency, a project-based funding to advance French research.

REFERENCES

1. J. G. McNally, C. Preza, J.-A. Conchello, and L. J. Thomas, "Artifacts in computational optical-sectioning microscopy," J. Opt. Soc. Am. A **11**, 1056–1067 (1994).

2. J. G. McNally, T. Karpova, J. Cooper, and J. A. Conchello, "Three-dimensional imaging by deconvolution microscopy," Methods **19**, 373–385 (1999).
3. P. Sarder and A. Nehorai, "Deconvolution methods for 3-D fluorescence microscopy images," IEEE Signal Process. Mag. **23**, 32–45 (2006).
4. R. Neelamani, "ForWaRD: Fourier-wavelet regularized deconvolution for ill-conditioned systems," IEEE Trans. Signal Process. **52**, 418–433 (2004).
5. C. Vonesch and M. Unser, "A fast thresholded landweber algorithm for wavelet-regularized multidimensional deconvolution," IEEE Trans. Image Process. **17**, 539–549 (2008).
6. S. F. Gibson and F. Lanni, "Experimental test of an analytical model of aberration in an oil-immersion objective lens used in three-dimensional light microscopy," J. Opt. Soc. Am. A **9**, 154–166 (1992).
7. C. Preza and J.-A. Conchello, "Depth-variant maximum-likelihood restoration for three-dimensional fluorescence microscopy," J. Opt. Soc. Am. A **21**, 1593–1601 (2004).
8. J. G. Nagy and D. P. O'Leary, "Fast iterative image restoration with a spatially-varying PSF," Proc. SPIE **3162**, 388–399 (1997).
9. C. Preza and J.-A. Conchello, "Image estimation accounting for point-spread function depth-variation in three-dimensional fluorescence microscopy," Proc. SPIE **4964**, 135–142 (2003).
10. M. Arigovindan, J. Shaevitz, J. McGowan, J. W. Sedat, and D. A. Agard, "A parallel product-convolution approach for representing the depth varying point spread functions in 3D widefield microscopy based on principalcomponent analysis," Opt. Express **18**, 6461–6476 (2010).
11. J. W. Shaevitz and D. A. Fletcher, "Enhanced three-dimensional deconvolution microscopy using a measured depth-varying point-spread function," J. Opt. Soc. Am. A **24**, 2622–2627 (2007).
12. S. F. Gibson and F. Lanni, "Diffraction by a circular aperture as a model for three-dimensional optical microscopy," J. Opt. Soc. Am. A **6**, 1357–1367 (1989).
13. P. Török, P. Varga, Z. Laczik, and G. R. Booker, "Electromagnetic diffraction of light focused through a planar interface between materials of mismatched refractive indices: an integral representation," J. Opt. Soc. Am. A **12**, 325–332 (1995).
14. A. Chomik, A. Dieterlen, C. Xu, O. Haeberle, J. J. Meyer, and S. Jacquey, "Quantification in optical sectioning microscopy: a comparison of some deconvolution algorithms in view of 3D image segmentation," J. Opt. **28**, 225–233 (1997).
15. A. Diaspro, F. Federici, and M. Robello, "Influence of refractive-index mismatch in high-resolution three-dimensional confocal microscopy," Appl. Opt. **41**, 685–690 (2002).
16. O. Haeberlé, F. Bicha, C. Simler, A. Dieterlen, C. Xu, B. Colicchio, S. Jacquey, and M.-P. Gramain, "Identification of acquisition parameters from the point spread function of a fluorescence microscope," Opt. Commun. **196**, 109–117 (2001).
17. F. Aguet, D. Van de ville, and M. Unser, "An accurate PSF model with few parameters for axially shift-variant deconvolution," in *IEEE International Symposium on Biomedical Imaging: From Nano to Macro* (IEEE, 2008), pp. 157–160.
18. Z. Kam, B. Hanser, M. G. L. Gustafsson, D. A. Agard, and J. W. Sedat, "Computational adaptive optics for live three-dimensional biological imaging," Proc. Natl. Acad. Sci. U.S.A. **98**, 3790–3795 (2001).
19. B. M. Hanser, M. G. L. Gustafsson, D. A. Agard, and J. W. Sedat, "Phase-retrieved pupil functions in wide-field fluorescence microscopy," J. Microsc. **216**, 32–48 (2004).
20. J. B. de Monvel, E. Scarfone, S. Le Calvez, and M. Ulfendahl, "Image-adaptive deconvolution for three-dimensional deep biological imaging," Biophys. J. **85**, 3991–4001 (2003).
21. M. Von Tiedemann, A. Fridberger, M. Ulfendahl, I. Tomo, J. B. de Monvel, and J. B. De Monvel, "Image adaptive point-spread function estimation and deconvolution for in vivo confocal microscopy," Microsc. Res. Tech. **69**, 10–20 (2006).
22. S. X. Liao and M. Pawlak, "Image analysis with Zernike moment descriptors," in *1997 IEEE Canadian Conference on Electrical and Computer Engineering* (IEEE, 1997), Vol. 2, pp. 700–703.
23. C.-W. Chong, P. Raveendran, and R. Mukundan, "Translation invariants of Zernike moments," Pattern Recogn. **36**, 1765–1773 (2003).
24. A. Dieterlen, A. De Meyer, P. Kessler, B. Colicchio, and J. De Mey, "On the use of Zernike polynomials in PSF processing: 4-D wide field fast microscopy images deconvolution," presented at the International Conference Focus on Microscopy 2005, Jena, Germany (March 20–23, 2005).
25. A. De Meyer, "Contribution à l'amélioration des outils de restauration d'image et de caractérisation de l'instrument en microscopie 3D par fluorescence," Ph.D. dissertation (Université de Mulhouse, 2008).
26. N. Becherer, H. Jodicke, G. Schlosser, J. Hesser, F. Zeilfelder, and R. Manner, "On soft clipping of Zernike moments for deblurring and enhancement of optical point spread functions," Proc. SPIE **6065**, 60650C-11 (2006).
27. O. Haeberlé, "Focusing of light through a stratified medium: a practical approach for computing microscope point spread functions. Part I: conventional microscopy," Opt. Commun. **216**, 55–63 (2003).
28. M. R. Teague, "Image analysis via the general theory of moments*," J. Opt. Soc. Am. **70**, 920–930 (1980).
29. M. Pawlak and S. X. Liao, "On the recovery of a function on a circular domain," IEEE Trans. Inf. Theory **48**, 2736–2753 (2002).
30. A.-R. Mohammed and J. Yang, "Practical fast computation of Zernike moments," J. Comp. Sci. Technol. **17**, 181–188 (2002).
31. J. Gu, H. Z. Shu, C. Toumoulin, and L. M. Luo, "A novel algorithm for fast computation of Zernike moments," Pattern Recogn. **35**, 2905–2911 (2002).